Form finding in elastic gridshells

Form finding in elastic gridshells

Changyeob Baek[a,1], Andrew O. Sageman-Furnas[b,1], Mohammad K. Jawed[a], and Pedro M. Reis[a,c,d,2]

[a]Department of Mechanical Engineering, Massachusetts Institute of Technology, Cambridge, MA 02139; [b]Institute for Numerical and Applied Mathematics, University of Goettingen, 37073 Goettingen, Germany; [c]Department of Civil and Environmental Engineering, Massachusetts Institute of Technology, Cambridge, MA 02139; and [d]Flexible Structures Laboratory, Ecole Polytechnique Fédérale de Lausanne, Lausanne CH-1015, Switzerland

Edited by David A. Weitz, Harvard University, Cambridge, MA, and approved November 20, 2017 (received for review August 4, 2017)

Elastic gridshells comprise an initially planar network of elastic rods that are actuated into a shell-like structure by loading their extremities. The resulting actuated form derives from the elastic buckling of the rods subjected to inextensibility. We study elastic gridshells with a focus on the rational design of the final shapes. Our precision desktop experiments exhibit complex geometries, even from seemingly simple initial configurations and actuation processes. The numerical simulations capture this nonintuitive behavior with excellent quantitative agreement, allowing for an exploration of parameter space that reveals multistable states. We then turn to the theory of smooth Chebyshev nets to address the inverse design of hemispherical elastic gridshells. The results suggest that rod inextensibility, not elastic response, dictates the zeroth-order shape of an actuated elastic gridshell. As it turns out, this is the shape of a common household strainer. Therefore, the geometry of Chebyshev nets can be further used to understand elastic gridshells. In particular, we introduce a way to quantify the intrinsic shape of the empty, but enclosed regions, which we then use to rationalize the nonlocal deformation of elastic gridshells to point loading. This justifies the observed difficulty in form finding. Nevertheless, we close with an exploration of concatenating multiple elastic gridshell building blocks.

elastic structures | gridshells | buckling | Chebyshev nets | mechanical instabilities

Camping tents create curved shell-like structures in three dimensions (3D) through elastic buckling of a network of rods. In the 1970s, the architectural community transferred this idea into the realm of large-scale construction (1) by introducing the concept of an elastic gridshell, a regular grid of elastic rods that is actuated into a shell-like structure by loading its extremities. Research has since focused mostly on case studies (1–3) and computational form finding of the static actuated geometry (4–6). Elastic gridshells fit with the recent trend in extreme mechanics to design through buckling, by harnessing the underlying geometry (7, 8). Examples of these geometry-driven structures range from microscopic buckling of a series of ribbons attached to a prestretched substrate (9) to macroscopic origami-inspired engineering (10, 11).

The buckled forms of elastic gridshells (Fig. 1*A*) suggest a nontrivial functional relationship between the initially flat, regular grid and the ensuing actuated geometry, making both forward and inverse design challenging tasks. This relationship juxtaposes rod elasticity and inextensibility, which are well understood in 1D as classical Euler's elastica (12), with a network of 2D constraints that oversee the emergence of a shell-like structure. This network can be modeled, on the one hand, from the perspective of interacting constrained elastica (13–15), an approach that is common in the study of random 3D polymer systems (16), but not as well explored for structured 2D networks. On the other hand, an elastic network can be modeled as a continuum of inextensible rods subjected to bending or shearing (17–20), which results in Euler–Lagrange equations but whose tractable solutions are often restricted to a plane or particular simple geometries. Instead of the variational approach, one can encode an elastic grid as a purely geometric object using the differential geometry of surfaces (21). This approach was taken by P. L. Chebyshev in the 1880s (22) while investigating the deformations of woven fabric. The resulting theory of smooth Chebyshev nets is an ongoing topic of research which is one of the central themes of our study.

Here, we combine both perspectives of an elastic gridshell as an ensemble of constrained elastica and a continuum of inextensible rods to provide a quantitative description of their behavior. We focus on rationalizing the design challenges that underlie the actuation process and the resulting shape. Our physical model implements a 2D network of inextensible elastic rods in a desktop-scale setting that allows for high-precision validation against numerical simulations and theory. For simulations, we extend the discrete elastic rod (DER) method (23, 24) to elastic gridshells. We find excellent agreement with experiments (Fig. 1), allowing us to explore the parameter space of a seemingly simple elastic gridshell. This exploration reveals the complexity of actuation and forward design, as well as the presence of multistability. We then interpret elastic gridshells as both a network of smooth rods and a continuum by finitely sampling a Chebyshev net. This perspective enables an inverse design process, whose results suggest that rod inextensibility—not elasticity—is primary in dictating the zeroth-order shape of an actuated elastic gridshell. Moreover, our combined perspective allows us to harness theorems about smooth Chebyshev nets to rationalize elastic gridshell shape. This leads to quantitative investigations of their nonlocal response to loading and provides justification of the difficulties in form finding. We, therefore, expose the geometry-driven nature of elastic gridshells.

Significance

Elastic gridshells arise from the buckling of an initially planar grid of rods. The interaction of elasticity and geometric constraints makes their actuated shapes difficult to predict using classical methods. However, recent progress in extreme mechanics reveals the benefits of structures that buckle by design, when exploiting underlying geometry. Here, we demonstrate the geometry-driven nature of elastic gridshells. We use a geometric model, originally for woven fabric, to rationalize their actuated shapes and describe their nonlocal response to loading. Validation is provided with precision experiments and rod-based simulations. The prominence of geometry in elastic gridshells that we identify should allow for our results to transfer across length scales from architectural structures to micro/nano–1-df mechanical actuators and self-assembly systems.

Author contributions: A.O.S.-F. and P.M.R. designed research; C.B., A.O.S.-F., and P.M.R. performed research; C.B., A.O.S.-F., M.K.J., and P.M.R. contributed new reagents/analytic tools; C.B. and A.O.S.-F. analyzed data; and C.B., A.O.S.-F., and P.M.R. wrote the paper.

The authors declare no conflict of interest.

This article is a PNAS Direct Submission.

[1]C.B. and A.O.S.-F. contributed equally to this work.

[2]To whom correspondence should be addressed. Email: pedro.reis@epfl.ch.

This article contains supporting information online at www.pnas.org/lookup/suppl/doi:10.1073/pnas.1713841115/-/DCSupplemental.

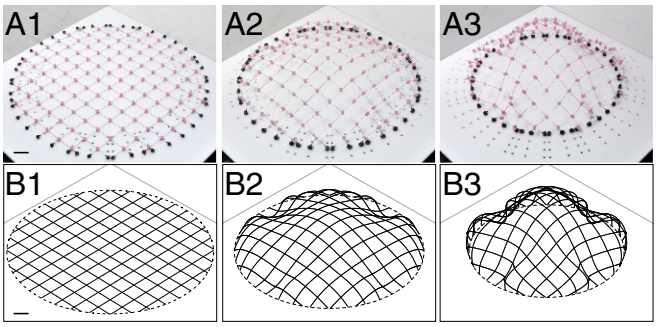

Fig. 1. (*A* and *B*) Actuation of an elastic gridshell from (*A*) experiments and (*B*) DER simulation. The edge points of a planar and unloaded footprint (*A1* and *B1*) are gradually moved toward a prescribed actuated boundary (*A2* and *B2*) to yield an actuated shape (*A3* and *B3*). (Scale bar, 20 mm.)

Anatomy and Actuation of an Elastic Gridshell

Our model system comprises a planar, completely unloaded footprint of elastic rods that is actuated by loading its extremities (Fig. 1 *A1*). A footprint is constructed from straight elastic rods that are assumed to be inextensible (*Materials and Methods*). First, two sets of parallel rods with spacing d are laid perpendicularly. Then, the points of contact between cross-laid rods are constrained by joints. A square grid results, where each empty unit cell is enclosed by four adjacent rod segments of length d. Finally, the square grid is cut along an original boundary that encloses the footprint. A footprint thus contains a region of square grid and a boundary layer of "legs" extending to edge points along the original boundary. Pinning these edge points onto an actuated boundary of smaller perimeter induces out-of-plane buckling. The ensuing 3D actuated form is dictated by a combination of the elastic deformation of the rods and the geometric constraints of the grid. Without joints, each rod would act as an independent Euler's elastica (12). Instead, the system behaves as a shell-like structure, whose shape, in contrast to a continuum shell, must be rationalized by resolving its actuated unit cells. We explored the form finding of elastic gridshells, using precision desktop-scale experiments (*Materials and Methods*). Elastomeric joints enforce positional constraints between cross-laid Nitinol rods, with negligible resistance to both shear of the unit cells and transport of twist along each rod. The superelastic nature of Nitinol ensures that the gridshell remains elastic throughout actuation. Pinned boundary conditions at the edge points are set by 3D-printed ball joints, which, for actuation, were manually fitted onto a series of laser-cut holes on the designated actuated boundary (Fig. 1*A*).

In parallel to the experiments, we performed numerical simulations using the DER method, which was originally developed in the computer graphics community for the realistic visualization of filamentous structures such as hair and fur (23, 24). More recently, DER has been shown to be remarkably predictive in engineering contexts to quantify large deformations of elastic rods (25). Our current implementation of DER simulates elastic gridshells using rods under Kirchhoff's assumptions, with the same physical parameters as in experiments. The positional constraints imposed by joints are modeled by stiff effective springs (*Materials and Methods*).

In Fig. 1 and Movie S1, we show representative examples, from both physical experiments (Fig. 1 *A1–A3*) and numerical simulations (Fig. 1 *B1–B3*), of a footprint with a circular original boundary, with radius $R_o = 126.0$ mm, that was gradually compressed to circular actuated boundaries with radii R_a [mm] $= \{126.0,\ 115.9,\ 94.5\}$. Excellent qualitative agreement is found between the two. As the actuation progresses, the height of the midsection increases and a dome-shaped gridshell emerges. We also consider noncircular boundaries.

Elastic Gridshells with Circular Boundaries

Even though the original and actuated boundaries in the example of Fig. 1 were both circular, the resulting actuated geometries were surprisingly complex (we expected to find entirely concave domes). This behavior is a signature of higher-order modes, which are known to arise in the theory of constrained elastica (13–15), and suggests the presence of multistability. Moreover, these complex geometries point to a nontrivial functional relationship between footprints and their actuated forms, which we address next.

In Fig. 2 *A1–A3*, we show three multistable states of the same elastic gridshell, in both experiment and simulation. The experimental state is represented by the positions of its joints (red solid circles) acquired via 3D laser scanning (*Materials and Methods*) and was obtained by manually point loading the actuated form and allowing it to snap into a new state. The corresponding multistable numerical solutions (solid lines) were computed by a jittering algorithm (*Materials and Methods*) and are in excellent quantitative agreement with experiments; the maximum joint positional mismatch is within two joint radii.

Given the accurate predictions from our simulations, we now rely on DER to systematically explore the parameter space of elastic gridshells with circular boundaries. The radius of the actuated boundary is set to $R_a = 0.75R_o$. To investigate boundary layer effects, we consider the longest "leg" in a footprint with n rods per direction, normalized by its unit cell spacing d; i.e., $\bar{L}_d = \frac{L}{d} = \frac{R_o}{d} - \frac{n-1}{2}$. We further enforce $\bar{L}_d > 0$ (otherwise, the number of rods would reduce to $n - 2$). In Fig. 2*B*, we show the

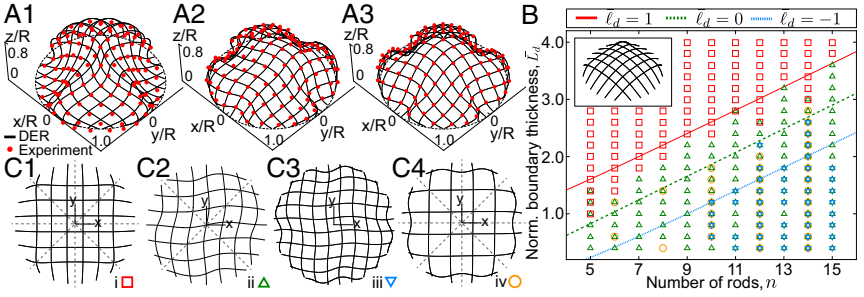

Fig. 2. Elastic gridshells with circular boundaries. (*A*) Multistable states of a circular elastic gridshell with $(\bar{L}_d, n) = (0.8, 12)$ observed from experiments (red solid circles) and simulations (black lines). (*B*) Phase diagram of elastic gridshells with circular boundaries. In addition to the three states in *A*, a convex dome-shaped state (*B*, *Inset*) is obtained by extending the legs. Each data point is obtained from DER simulations under a jittering procedure. (*C*) Four representative modes of the circular elastic gridshells with different symmetry properties.

resulting phase diagram in the $(\bar{L}_d, n)$ parameter space, where each footprint was actuated and subject to our jittering algorithm. We observe four qualitatively distinct states; examples are shown in Fig. 2 *C1–C4*. All footprints considered have four symmetry planes ($y = x$, $y = -x$, $x = 0$, and $y = 0$). State *i* retains full symmetry and involves only first-order rod buckling, resulting in concave domes. States *ii* and *iii* exhibit symmetry breaking and higher-order buckling; state *ii* retains only two symmetry planes while state *iii* retains only 90° rotational symmetry. In contrast, state *iv* also involves higher-order buckling but retains full symmetry.

We interpret the presence of multistability in Fig. 2*B* by considering the normalized length of the shortest leg; i.e., $\bar{\ell}_d = \frac{\ell}{d} = \left[\left(\frac{R_o}{d}\right)^2 - \left(\frac{n-1}{2}\right)^2\right]^{1/2} - \frac{n-1}{2}$. When $\bar{\ell}_d > 1$, joints still constrain the overall shape, but do not prevent all rods from exhibiting first-order buckling, and result in monostable concave domes. The onset of multistable states occurs for $\bar{\ell}_d \lesssim 1$. Note that, even though $\bar{L}_d \geq 0$, the quantity $\bar{\ell}_d$ can be nonpositive. We observe that states *iii* and *iv* start to appear for $\bar{\ell}_d \approx 0$, and they occur for almost all possible configurations when $\bar{\ell}_d \lesssim -1$.

Even though we got concave domes by increasing the footprint legs, the ensuing geometries were not hemispherical despite having circular boundaries. How can one obtain a hemispherical gridshell? Can we better understand the anisotropy induced by rod inextensibility?

Hemispherical Elastic Gridshells from Chebyshev Nets

In Fig. 3*A*, we show an experimental gridshell with $\lesssim$2% pointwise deviation from a hemisphere. The original boundary of its footprint is a rounded diamond (Fig. 3*B*, outermost curve). Recall from above that, by contrast, circular original boundaries produced complex, multistable geometries (Fig. 2*A*). We demonstrate how the continuum theory of Chebyshev nets (22, 26) can be used to rationally design and quantify the geometry of elastic gridshells, as in the example of Fig. 3*A*. Whereas a discrete analog of Chebyshev nets [which approximates all rod segments between joints by straight lines of the same length (27)] has previously been used for this class of problems (1, 5, 6), we emphasize the relationship to smooth Chebyshev nets. This perspective offers three benefits for elastic gridshells: (*i*) a precise method to quantify the accuracy of the actuated forms vis-à-vis the original target designs, (*ii*) a quantitative characterization of the geometry at the level of the curved unit cells, and (*iii*) a rationale for the nonlocal response to loading.

A Review of Chebyshev Nets. Before continuing with our own work, we provide a brief review of a smooth Chebyshev net, defined as a smooth parameterized surface patch $\mathbf{C} : D \subset \mathbb{R}^2 \to \mathbb{R}^3$, from a domain D in 2D with its orthogonal coordinate system (u, v) to a smooth surface in 3D, under the condition $\|\partial\mathbf{C}/\partial u(u,v)\| = \|\partial\mathbf{C}/\partial v(u,v)\| = 1$. Physically, this condition corresponds to inextensibility of the rods along the two initially perpendicular parameter directions. We regard $\mathbf{C}$ as the deformation of a continuum planar domain of inextensible rods into a surface, during which crossing rods shear freely at joints. The shear angle function $0 < \omega(u,v) < \pi$ turns the unit tangent vector $\partial\mathbf{C}/\partial u$ into $\partial\mathbf{C}/\partial v$.We focus on smooth Chebyshev nets that do not have singularities; i.e., no rod collapses onto another with $\omega \in \{0, \pi\}$.

A smooth Chebyshev net exists locally around each point of a surface (18, 28), but a global obstruction constraining the curvature arises from the necessary Gauss equation (21)

$$-\mathcal{K}(u,v)\sin\omega(u,v) = \frac{\partial^2}{\partial u \partial v}\omega(u,v), \qquad [1]$$

which enforces a strict coupling between shear and Gauss curvature, $\mathcal{K}(u,v)$. As rods shear, infinitesimal squares deform into rhombi, and the surface area element is $\mathrm{d}A = \sin\omega\,\mathrm{d}u\mathrm{d}v$. Integrating Eq. **1** (with respect to u and v) over an axis-aligned rectangle (denoted as $\square$) yields a seminal result due to Hazzidakis (ref. 29; see also ref. 21): The integrated Gauss curvature of each deformed rectangle depends only on its four interior angles $0 < \alpha_i < \pi$,

$$\int_{\mathbf{C}(\square)} \mathcal{K}(u,v)\,dA = 2\pi - \sum_{i=1}^{4}\alpha_i, \qquad [2]$$

so the maximum integrated Gauss curvature of every region enclosed by four rods is 2π. Due to this inability to encode regions with high curvature, finding a singularity-free smooth Chebyshev net that lies on, or approximates to, an entire arbitrary target shape is challenging and the topic of much ongoing theoretical (30–34) and applied research (35–37). The key idea is to carefully design the domain, which translates into the footprint of an elastic gridshell.

Footprint and Actuation Ansatzes from a Chebyshev Net. We use smooth Chebyshev nets as educated guesses (ansatzes) for the design of elastic gridshells that provide solutions under the nontrivial inextensibility conditions, but neglect bending.

Formalizing an elastic gridshell, we define its footprint $\mathcal{F}^d_{\mathbf{b}}$ by an enclosing original boundary $\mathbf{b}$, which cuts an infinite square grid of spacing d. A correspondence $\mathbf{g} : \mathbf{b} \to \mathbf{a}$ between positions along $\mathbf{b}$ and an actuated boundary $\mathbf{a}$ determines the location of the pinned edge points. The resulting actuated elastic gridshell

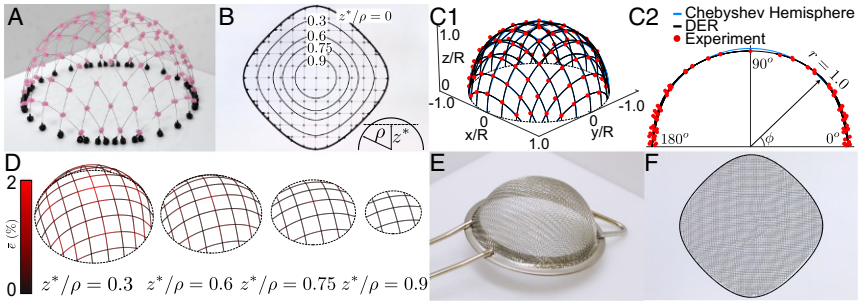

Fig. 3. Hemispherical elastic gridshells from Chebyshev's hemisphere ansatz. (*A*) Photograph of a nearly hemispherical gridshell. (*B*) Boundary of the hemisphere domain (outermost contour) and spherical caps (five inner contours) obtained by cutting with planes (*Inset*). (*C*) Positions of the joints (red solid circles; 3D scanning), along with the corresponding DER simulation (black solid lines) and the *d*-sampled Chebyshev net (blue solid lines). (*D*) Spherical-cap elastic gridshells obtained from DER simulations, whose footprints are shown in *B*. Colorbar represents deviation from the *d*-sampled Chebyshev net normalized by the radius of the sphere, $\bar{e} = \Delta/\rho$. (*E* and *F*) A household strainer of $z^*/\rho = 0.28$ (*E*) and its flattened 2D domain (*F*), showing excellent agreement with a Chebyshev domain (solid line).

is represented by $\mathbf{G}$: $\mathcal{F}_{\mathbf{b}}^{d} \rightarrow \mathbb{R}^3$. A specific Chebyshev net $\mathbf{C}$ is regarded as a viable ansatz if, for each position $b \in \mathbf{b}$ of the original boundary that maps to an actuated position $a \in \mathbf{a}$, we have $\mathbf{C}(b) = \mathbf{g}(b) = a$. Determining a viable ansatz for an elastic gridshell involves three steps. First, we specify an actuated boundary $\mathbf{a}$ in the Chebyshev net surface. Second, we compute the original boundary in the domain by solving for the contour $\mathbf{C}(\mathbf{b}) = \mathbf{a}$. Third, we fix $d > 0$ to determine the footprint $\mathcal{F}_{\mathbf{b}}^{d}$ enclosed by $\mathbf{b}$.

Our ansatz procedure does not consider the pinned boundary conditions on the actuated boundary, which lead to higher-order constraints from variational considerations of the bending energy (19). Therefore, we quantify deviations, as follows, to attest the accuracy of viable Chebyshev net ansatzes. We first restrict $\mathbf{C}$ to points of the footprint $\mathcal{F}_{\mathbf{b}}^{d}$ (d sampling of the Chebyshev net). Then, for each footprint point, $x \in \mathcal{F}_{\mathbf{b}}^{d}$, we define $\Delta(x) = \|\mathbf{C}(x) - \mathbf{G}(x)\|$, the pointwise distance between an actuated elastic gridshell and a d-sampled viable ansatz.

Elastic Gridshells That Resemble Spherical Caps. With the goal of designing hemispherical and spherical-cap gridshells, we consider Chebyshev's hemisphere $\mathbf{C}_h$ (22, 26, 38, 39) (see *SI Appendix, S1. Hemispherical Ansatz* for details on its construction). We then use $\mathbf{C}_h$ as a viable ansatz by solving for the original boundary (shown as the outermost contour of Fig. 3*B*) that corresponds to an actuated boundary of the equator and fixing a unit cell spacing $d = 20$ mm. This yields a footprint $\mathcal{F}_{\mathbf{b}}^{d}$, which is then actuated into an elastic gridshell $\mathbf{G}_h$. In Fig. 3 *C1* and *C2*, we quantify the deviation between the computed d sampling of $\mathbf{C}_h$ (blue curves) and the elastic gridshells corresponding to $\mathbf{G}_h$ obtained from both DER simulations (black curves) and experiments (red solid circles). A visual comparison is shown in Fig. 3 *C1*, while Fig. 3 *C2* plots the data using spherical coordinates without longitudinal information (radius r, latitude ϕ); there is excellent agreement between theory, simulations, and experiments. Hereafter, we compare a viable ansatz only with a DER actuated elastic gridshell. Quantitatively, we find that there is $\lesssim 2\%$ deviation between the d-sampled $\mathbf{C}_h$ and the DER elastic gridshell $\mathbf{G}_h$ (using Δ as introduced above).

To further affirm the strength of our ansatz protocol, we use the same $\mathbf{C}_h$ to compute original boundaries of footprints for other spherical caps. Circles of latitude are used to slice the hemisphere by planes at varying heights ($0 \leq z^*/\rho < 1$) and understood as actuated boundaries $\mathbf{a}_{z^*}$. Note that ρ is the fixed radius of the sphere and agrees with the radius of $\mathbf{a}_{z^*}$ only when $z^*/\rho = 0$ (entire hemisphere). After fixing $d = 20$ mm, the corresponding original boundaries $\mathbf{b}_{z^*}$ (Fig. 3*B*) yield a series of actuated elastic gridshells $\mathbf{G}_{z^*}$. In Fig. 3*D*, we quantify the resulting deviations. As z^*/ρ increases, the deviation decreases from 1.87% ($z^*/\rho = 0.3$) to 0.17% ($z^*/\rho = 0.9$). This agreement is surprising since the smaller footprints contain even fewer rods; a continuum Chebyshev net ansatz may continue to be valid even for very coarse footprints within the limits of our inextensibility assumptions, whose applicability is investigated in *SI Appendix, S5. Inextensibility Limits of Elastic Gridshells*. To emphasize the geometric nature of these results, we considered a common household strainer (Fig. 3*E*), which also forms a spherical cap from a network of plastic inextensible rods. Interestingly, its flattened shape (after being cut along its "actuated boundary" rim) shows excellent agreement with a corresponding "original boundary" from $\mathbf{C}_h$ (Fig. 3*F*), thereby pointing to the generality of our framework.

Deformation of the Unit Cells and Nonlocal Response

Success in deriving elastic gridshells from smooth Chebyshev net ansatzes suggests broader applicability. We now use smooth Chebyshev net theory to rationalize the shape of elastic gridshells. In particular, we introduce a notion of integrated Gauss curvature that relates directly to the shearing of the actuated unit cells. Subsequently, we use this notion to explore the nonlocal and highly anisotropic response of elastic gridshell systems under point-load indentation.

Integrated Gauss Curvature per Unit Cell. Even though the surface of a unit cell is ill-defined, it does have well-defined crossing angles at its joints. Using Hazzidakis' result, Eq. **2**, for each unit cell of an actuated gridshell, we define its integrated Gauss curvature as $K^{\square} = 2\pi - \sum_{i=1}^{4} \alpha_i$. If the enclosing rods of an actuated unit cell were to lie along geodesics, then the Gauss–Bonnet theorem (21) would state that the integrated Gauss curvature of the enclosed region would be $\sum_{i=1}^{4} \alpha_i - 2\pi$, exactly the negative of our quantity $K^{\square}$. We will see that, generally, $K^{\square}$ carries the sign matching our intuition, implying that we do not interpret elastic gridshell rods as lying along geodesics of an underlying surface.

Next, we evaluate the validity of the notion of integrated Gauss curvature, $K^{\square}$, to design and describe elastic gridshells. We study viable ansatzes from surfaces of constant (*i*) positive, (*ii*) zero, and (*iii*) negative Gauss curvature, for which we use, respectively, (*i*) Chebyshev's hemisphere $\mathbf{C}_h$, (*ii*) half a circular cylinder parameterized by helices $\mathbf{C}_c$, and (*iii*) half an analytic parameterization for a pseudosphere of revolution $\mathbf{C}_p$. The latter two are special cases of Chebyshev nets on surfaces of revolution (40) (*SI Appendix, S2. Cylindrical and Pseudospherical Ansatzes*).

In Fig. 4*A*, *Left* to *Right*, we show that the obtained elastic gridshells closely resemble their ansatz d samplings, with only small deviations. In Fig. 4*B*, we plot $K^{\square}$ vs. the centroid of its four vertices in space along the shown axis. We find that $K^{\square}$ matches our expectation, with actuated unit cells that visually resemble regions of positive, zero, and negative curvature having an integrated Gauss curvature that is correctly signed. Our chosen ansatzes do not incorporate bending, which impacts the shape of the actuated forms. Most prominently, Fig. 4*A*, *Right* shows $\mathbf{G}_p$ protruding above its negatively curved Chebyshev ansatz $\mathbf{C}_p$ immediately after leaving its actuated boundary, before dipping in the middle. This behavior is consistent with a change from

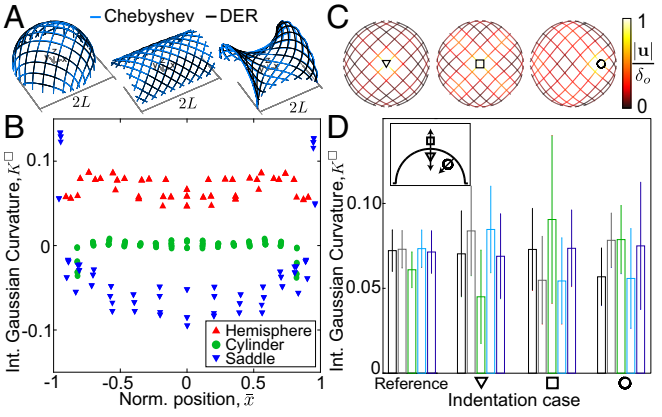

Fig. 4. Notion of integrated Gauss curvature. (*A*) Elastic gridshells (DER simulation; black solid lines) and their *d*-sampled Chebyshev ansatzes (blue solid lines), which are from *Left* to *Right*, respectively, a hemisphere, a cylinder, and a saddle (each with half-span *L*). (*B*) Distribution of $K^{\square}$, the integrated Gauss curvature of a unit cell obtained from Eq. **2**, for three elastic gridshells. Each unit cell is positioned by its normalized centroid $\bar{x} = x/L$. (*C*) Three indentation cases of an actuated hemispherical gridshell: (*Left*) inward and (*Center*) outward normal displacement at the north pole and (*Right*) inward displacement at $\pi/4$ latitude and longitude. The normalized displacement field is $|\mathbf{u}|/\delta_o$. (*D*) Binned $K^{\square}$ for *C* (*Left* to *Right*). Averages (bins) and standard deviations (error bars) show the spatial heterogeneity (i.e., nonlocality) of the shearing response.

positive to negative curvature and is reflected in the distribution of $K^{\square}$, which derives from the actuated elastic gridshell itself, not a choice of viable ansatz.

We therefore find $K^{\square}$ to be an excellent proxy for the curvature of actuated unit cells and its definition in terms of crossing angles at joints provides a way for us to rationalize the distribution of shearing across an elastic gridshell.

Nonlocal Response to Point Loading. The quantity $K^{\square}$ not only describes the geometry of elastic gridshells, but also enables us to interpret and quantify their nonlocal response under point loads. Given the hyperbolic nature of the underlying Gauss equation, Eq. **1**, the rods can be regarded as characteristics, regularized by bending energy, that act as "highways of deformation." As such, we expect nonlocal behavior to be prevalent in elastic gridshells. In contrast, similar loading of a thin isotropic continuum shell leads to a deformation that is local to a small spherical cap (41–43).

We subject an actuated hemispherical elastic gridshell $\mathbf{G}_h$ to three types of point loading: (*i* and *ii*) inward (*i*) and outward (*ii*) normal displacement at the north pole and (*iii*) inward displacement at $\pi/4$ latitude and longitude. The magnitude of the indentation was chosen to be $\delta_o = 0.1\rho$. In Fig. 4*C*, we present the top view of these loaded elastic gridshells obtained with DER simulations and quantify the displacement from the unloaded, but actuated, state. Corresponding experimental elastic gridshells under manual indentation are shown in Movie S2. The response for all three loading cases of the hemispherical elastic gridshell is strikingly nonlocal. Case *i* introduces not only a local dimpled cap but also displacements at the midpoints and corners of the largest concentric curved rhombus, nearly reaching the boundary. Case *ii* causes the center pair of rods to approach their inextensibility limits, forcing displacements to reach down to the equator. Case *iii* introduces displacement in a series of concentric curved rhombi that span the system.

This nonlocal response can further be rationalized using $K^{\square}$. Movies S3–S5 present the time evolution of the spatial distribution of $K^{\square}$ for the above indentation cases *i*–*iii*. Each actuated unit cell is segmented by the centroid of its vertices along the axis shown in Fig. 4*A*, *Left* (total length $2L$). In Fig. 4*D*, as a snapshot, we plot the spatial average of $K^{\square}$ vs. bins of size $0.4/L$. The SD within a bin measures the spatial heterogeneity of the curvature carried by each quad. The unindented gridshell configuration is treated as reference. Upon indentation (in all three cases), the shear response is highly nonlocal, and the spatial distribution of $K^{\square}$ changes along its entire extent (Movies S3–S5). Interestingly, as indicated by horizontal lines in Movies S3–S5, the total integrated Gauss curvature (sum of all $K^{\square}$) remains constant throughout the indentation. This result reinforces that $K^{\square}$ is a valid reflection (beyond shearing) of integrated Gauss curvature. Moreover, a constant total $K^{\square}$ establishes that nonlocality in elastic gridshells is related to the regions enclosed by rods.

Assembling with Building Blocks

Finally, we seek to assemble building blocks into more complex structures. Our idea is to concatenate both individual footprints and in-plane actuated boundaries, which reduces the task of directly tackling a full target design. In Fig. 5 *A1*–*A3*, we present three examples of building blocks: a quarter-sphere, a cylinder, and a saddle. These building blocks are similar to the solutions in Fig. 4*A*, but their footprints and corresponding actuated boundaries have been strategically pruned at connection sites, where cross-laid rods form a series of v-shaped notches. This pruning ensures smooth assembly, with moderate deviation between the rod positions and tangents. For example, we pruned the building blocks in Fig. 5 *A1*–*A3* so that connection sites lie on half-circles of similar radii, which also removed the saddle's boundary rings (*SI Appendix, S2. Cylindrical and Pseudospherical Ansatzes*).

Two example geometries are targeted: a stadium (central cylinder capped by quarter-spheres) and a peanut (central saddle capped by quarter-spheres). The concatenated footprints, together with their actuated boundaries, are provided in Fig. 5 *B1* and *B2*. The resulting actuated geometries are shown in Fig. 5 *C1* and *C2*, where the building blocks (colored lines) are superposed onto the actuated assemblage elastic gridshells obtained from the DER (black lines). We find excellent qualitative agreement between building blocks and assemblages. In Fig. 5*D*, we present an experimental peanut-shaped elastic gridshell obtained from the footprint in Fig. 5 *B2*. In Fig. 5*E* we overlay the digitized experimental joint positions (red solid circles; *Materials and Methods*) with the DER simulation (black solid lines), which again exhibit excellent agreement; the maximum joint positional mismatch is within two joint radii.

Conclusion

We systematically explored elastic gridshells by combining theory with numerical and physical experiments. The design space of elastic gridshells with circular boundaries revealed a nontrivial relationship between flat and actuated geometries, as well as the possibility of multistability. We then turned to the role of inextensibility in the footprint design and created hemispherical elastic gridshells from a Chebyshev ansatz. The excellent agreement between Chebyshev's hemisphere and the resulting elastic gridshells motivated our further use of this theory. Using the formula of Hazzidakis, Eq. **2**, we quantified the intrinsic shape of the empty unit cells. This justified the difficulty in bottom–up form finding by providing a quantification of the nonlocal response of elastic gridshells. Nevertheless, we briefly suggested an approach to more targeted design through elastic gridshell building blocks.

Our investigations revealed the geometry-driven nature of elastic gridshells by merging the two perspectives of both an elastic gridshell as a finite network of elastic rods and a continuum of inextensible rods. This suggests that elastic gridshells, beyond their current use at the macroscale, may scale down to micro- or nanolength scales, where complex geometries arising from simple actuation have had exciting applications (9). In particular, exploring 1-df actuation techniques may lead to new modes of self-assembly. Complementing these explorations, one can move beyond our purely geometric treatment of elastic gridshells and focus on their mechanical and scale-dependent aspects, e.g., through the use of twist-transmitting joints, shear-resisting joints, or rods of nonlinear materials. The numerical framework we introduced, together with its excellent agreement with experiments, provides a foundation from which to build.

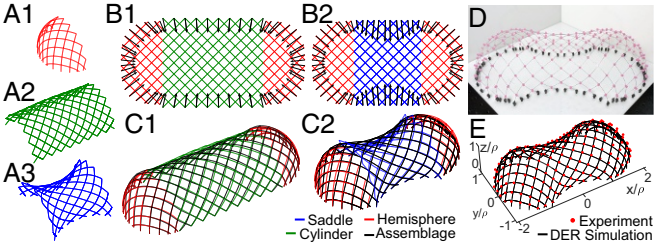

Fig. 5. Elastic gridshells from building blocks. (*A*) Pruned elastic gridshell building blocks: (*A1*) hemisphere, (*A2*) cylinder, and (*A3*) saddle. (*B* and *C*) Comparison of concatenated elastic gridshell assemblage (black solid lines) and its building blocks (colored solid lines) for (*B1* and *C1*) stadium (*A1-A2-A1*) and (*B2* and *C2*) peanut (*A1-A3-A1*). (*D*) Photograph of a peanut-shaped elastic gridshell. (*E*) Positions of the joints (red solid circles; 3D scanning), along with the corresponding DER simulation (black solid lines).

ENGINEERING

Materials and Methods

Fabrication of Elastic Gridshells and Their 3D Imaging. A square grid ($d = 20$ mm) of grooves (depth $t_g = 500$ μm) was etched onto an acrylic plate, and holes (diameter $D_r = 3$ mm) were laser cut at the intersections. Nitinol rods (diameter $D_r = 254$ μm and Young's modulus $E_r = 83$ GPa) were placed onto the positioning grooves of the acrylic plate and the holes served to cast vinylpolysiloxane (VPS) cylindrical joints (Young's modulus $E_j = 0.23 \pm 0.01$ MPa, diameter $D_j = 3$ mm, height $H_j = 5$ mm). After the joints cured, the grid was cut along the original boundary and a speck of liquid glue (Loctite) was applied at each joint to prevent sliding. The 3D-printed ball joints (diameter $D_b = 4$ mm) were attached at the edge-point extremities of each rod and manually fixed onto the laser-cut holes along the actuated boundary, resulting in the 3D actuated form (Movie S4). Actuated forms were digitized using a 3D laser scanner (NextEngine), with a resolution of 100 μm. Partly because the diameter of rods was too small to be scanned and partly because the Nitinol rods reflect the laser beam away, only the joints could be successfully scanned, each yielding a point cloud. The scanned points were clustered by proximity and then averaged to obtain each joint position.

DER Simulations and Jittering Algorithm. A detailed account of DERs is found in refs. 23 and 24, with further details provided in *SI Appendix, S4. Numerical Simulations*. The DER method derives equations of motion using the discretized geometry and is well suited for problems involving elastic rod-like structures under geometrically nonlinear deformations. Our implementation generates discretized geometry with joint constraints (modeled as stiff effective springs) according to an input footprint. To explore multistability for elastic gridshell domes, we applied a jittering algorithm to each configuration. Partially actuated forms were subjected to an "artificial gravitational field" at different levels of intensity. The force field was removed and actuation progressed until the final actuated boundary was reached. The resulting actuated forms were classified by symmetry and rod-buckling modes, as discussed in the main text.

ACKNOWLEDGMENTS. We thank Laelia Kim-Lan Vaulot for help with preliminary experiments. This work was supported by the National Science Foundation, Faculty Early Career Development Program (CAREER) CMMI-1351449. A.O.S.-F. was partially supported by the Deutsche Forschungsgemeinschaft Collaborative Research Center Transregio 109 "Discretization in Geometry and Dynamics."

1. Hennicke J, et al. (1974) *Grid Shells (IL 10)* (Institute for Lightweight Structures, Stuttgart).
2. Baverel O, Caron JF, Tayeb F, Peloux LD (2012) Gridshells in composite materials: Construction of a 300 m^2 forum for the Solidays' festival in Paris. *Struct Eng Int* 22:408–414.
3. Quinn G, Gengnagel C (2014) A review of elastic grid shells, their erection methods and the potential use of pneumatic formwork. *Mobile and Rapidly Assembled Structures IV*, eds De Temmerman N, Brebbia CA (WIT Press, Southampton, UK), pp 129–145.
4. Bulenda T, Knippers J (2001) Stability of grid shells. *Comput Struct* 79:1161–1174.
5. Hernández EL, Sechelmann S, Rörig T, Gengnagel C (2013) Topology optimisation of regular and irregular elastic gridshells by means of a non-linear variational method. *Advances in Architectural Geometry 2012*, eds Hesselgren L, et al. (Springer, Vienna), pp 147–160.
6. Lefevre B, Douthe C, Baverel O (2015) Buckling of elastic gridshells. *J IASS* 56:153–171.
7. Reis PM (2015) A perspective on the revival of structural (In)stability with novel opportunities for function: From buckliphobia to buckliphilia. *J Appl Mech* 82:111001.
8. Reis P, Jaeger H, van Hecke M (2015) Designer matter: A perspective. *Extreme Mech Lett* 5:25–29.
9. Xu S, et al. (2015) Assembly of micro/nanomaterials into complex, three-dimensional architectures by compressive buckling. *Science* 347:154–159.
10. Filipov ET, Tachi T, Paulino GH (2015) Origami tubes assembled into stiff, yet reconfigurable structures and metamaterials. *Proc Natl Acad Sci USA* 112:12321–12326.
11. Reis PM, Jiménez FL, Marthelot J (2015) Transforming architectures inspired by origami. *Proc Natl Acad Sci USA* 112:12234–12235.
12. Euler L, Carathéodory C (1952) *Methodus Inveniendi Lineas Curvas Maximi Minimive Proprietate Gaudentes Sive Solutio Problematis Isoperimetrici Latissimo Sensu Accepti* (Birkhäuser, Basel). Latin.
13. Roman B, Pocheau A (2002) Postbuckling of bilaterally constrained rectangular thin plates. *J Mech Phys Sol* 50:2379–2401.
14. Miller J, et al. (2015) Buckling of a thin elastic rod inside a horizontal cylindrical constraint. *Extreme Mech Lett* 3:36–44.
15. Miller J, et al. (2015) Buckling-induced lock-up of a slender rod injected into a horizontal cylinder. *Int J Sol Struct* 72:153–164.
16. Broedersz CP, MacKintosh FC (2014) Modeling semiflexible polymer networks. *Rev Mod Phys* 86:995–1036.
17. Rivlin RS (1955) Plane strain of a net formed by inextensible cords. *Indiana U Math J* 4:951–974.
18. Pipkin AC (1984) Equilibrium of Tchebychev nets. *Arch Ration Mech An* 85:81–97.
19. Wang WB, Pipkin AC (1986) Inextensible networks with bending stiffness. *Q J Mech Appl Math* 39:343–359.
20. Wang WB, Pipkin AC (1987) Plane deformations of nets with bending stiffness. *Acta Mech* 65:263–279.
21. Stoker JJ (1969) *Differential Geometry* (Wiley, New York).
22. Tschebyscheff PL (1878) *Sur la coupe des vêtements [On the cutting of garments]* (Association Française pour l'Avancement des Sciences, Paris), pp 154–155.
23. Bergou M, Wardetzky M, Robinson S, Audoly B, Grinspun E (2008) Discrete elastic rods. *ACM Trans Graph* 27:63.
24. Bergou M, Audoly B, Vouga E, Wardetzky M, Grinspun E (2010) Discrete viscous threads. *ACM Trans Graph* 29:116.
25. Jawed MK, Da F, Joo J, Grinspun E, Reis PM (2014) Coiling of elastic rods on rigid substrates. *Proc Natl Acad Sci USA* 111:14663–14668.
26. Chebyshev PL (1946) On the cutting of garments. *Uspekhi Mat Nauk* 1:38–42.
27. Bobenko AI, Pinkall U (1996) Discrete surfaces with constant negative Gaussian curvature and the Hirota equation. *J Diff Geom* 43:527–611.
28. Bianchi L (1902) *Lezioni di Geometria Differenziale* (Spoerri, Pisa, Italy), 2nd Ed, Vol 1–2. Italian.
29. Hazzidakis JN (1880) Über einige Eigenschaften der Flächen mit constantem Krümmungsmaass. *J Reine Angew Math* 1880:68–73. German.
30. Bakelman IY (1965) Chebyshev networks in manifolds of bounded curvature. *Trudy Matematicheskogo Instituta im VA Steklova* 76:124–129.
31. Samelson SL (1991) Global Tchebychev nets on complete two-dimensional Riemannian surfaces. *Arch Ration Mech An* 114:237–254.
32. Samelson SL, Dayawansa WP (1995) On the existence of global Tchebychev nets. *T Am Math Soc* 347:651–660.
33. Burago YD, Ivanov SV, Malev SG (2007) Remarks on Chebyshev coordinates. *J Math Sci* 140:497–501.
34. Masson Y, Monasse L (2016) Existence of global Chebyshev nets on surfaces of absolute Gaussian curvature less than 2 pi. *J Geom* 108:25–32.
35. Robertson RE, Hsiue ES, Sickafus EN, Yeh GSY (1981) Fiber rearrangements during the molding of continuous fiber composites. I. Flat cloth to a hemisphere. *Polym Composite* 2:126–131.
36. Aono M, Breen DE, Wozny MJ (2001) Modeling methods for the design of 3D broadcloth composite parts. *Comput Aided Des* 33:989–1007.
37. Garg A, et al. (2014) Wire mesh design. *ACM Trans Graph* 33:1–12.
38. Samelson SL (1991) Tchebychev nets on spheres. *Q Appl Math* 49:11–18.
39. Ghys É (2011) Sur la coupe des vêtements: Variation autour d'un thème de Tchebychev. *Enseign Math* 57:165–208. French.
40. Voss A (1882) Über ein neues Prinzip der Abbildung krummer Oberflächen. *Math Ann* 19:1–26. German.
41. Pogorelov AV (1988) *Bendings of Surfaces and Stability of Shells* (Am Math Soc, Providence, RI), Vol 72.
42. Vella D, Ajdari A, Vaziri A, Boudaoud A (2011) Wrinkling of pressurized elastic shells. *Phys Rev Lett* 107:174301.
43. Nasto A, Ajdari A, Lazarus A, Vaziri A, Reis PM (2013) Localization of deformation in thin shells under indentation. *Soft Matter* 9:6796–6803.